

An Efficient and Robust Object-Level Cooperative Perception Framework for Connected and Automated Driving

Zhiying Song, Fuxi Wen, *Senior Member, IEEE*, Hailiang Zhang and Jun Li

Abstract—Cooperative perception is challenging for connected and automated driving because of the real-time requirements and bandwidth limitation, especially when the vehicle location and pose information are inaccurate. We propose an efficient object-level cooperative perception framework, in which data of the 3D bounding boxes, location, and pose are broadcast and received between the connected vehicles, then fused at the object level. Two Iterative Closest Point (ICP) and Optimal Transport theory-based matching algorithms are developed to maximize the total correlations between the 3D bounding boxes jointly detected by the vehicles. Experiment results show that it only takes 5ms to associate objects from different vehicles for each frame, and robust performance is achieved for different levels of location and heading errors. Meanwhile, the proposed framework outperforms the state-of-the-art benchmark methods when location or pose errors occur.

Index Terms—Cooperative perception, vehicle-to-vehicle, location error, heading error, optimal transport.

I. INTRODUCTION

Automated driving relies on the accurate perception of the surrounding vehicles and dynamic environment. However, single automated vehicle is limited by the physical capabilities (*e.g.*, detection range) of the on-board sensors, this might cause traffic safety and efficiency issues. To extend the boundary of single vehicle, the connected automated vehicles (CAV) becomes a promising paradigm recent years [1].

CAVs are connected with vehicle-to-vehicle (V2V) or vehicle-to-everything (V2X) and sense the surrounding environments through multi agent cooperation. In practice, the effectiveness of cooperative perception hinges on two aspects: 1) real-time and faithful data transmission within the limited network bandwidth, and 2) robust information aggregation under highly dynamic and noisy environments.

The primary bottleneck for cooperative perception is the sharing of precise data with low latency and low communication burden [2]. Generally, sharing raw data provides the best performance because of the slightest information loss. But it can easily overload the communication network with heavy data loads. As a trade-off, features extracted from the raw data by deep neural networks can reduce the amount of data

to be shared and simultaneously maintain a relatively good data fusion performance. To further reduce the communication load, sharing fully processed data, such as the detected objects, takes fewer communication resources. Transmitting more data results in an increase in delay and communication burden. In this paper, we opt to fuse data from different CAVs at the object level, *i.e.*, share data after processing (*i.e.*, 3D bounding boxes, location and pose information) on the local CAVs. This minimizes the burden on the communication network, allowing for rapid processing, and it also reduces the sensitivity of the cooperative perception system to the loss of information. Most importantly, it doesn't rely on the type of connected agents and on-board sensors, it also has no requirement of strong computational capacity. This makes it a general method to be applied in multiple scenarios.

The second challenge is the robust information combination in highly dynamic and noisy environments. Cooperative perception is a difficult time-varying task working in the context of sensor noise, position errors and even malicious attacks. Nevertheless, most of the available studies concentrate on ideal traffic environments and do not account for potential errors in the system that poses significant threats to road safety [3]. For cooperative perception at the object level, to reinforce the perception performance of the Ego vehicle that receives and aggregates messages from others, data received from other CAVs must first be converted to Ego coordinates. In reality, the transformation matrices are estimated from sensor measurements, such as global positioning system (GPS), real-time kinematic (RTK) and inertial measurement unit (IMU), with limited resolution and accuracy. Therefore, the estimated transformation matrix shared among the CAVs is inaccurate. In addition to low fidelity, the location and pose data transmitted via the network can be lost or deliberately revised. The failure of cooperation caused by these reasons could lead to serious road safety consequences as shown in Fig. 1.

For these purposes, our paper focuses on the problem of cooperative perception at the object level with inaccuracies in the received location and pose information. To the best of our knowledge, most of the existing V2V-based cooperative perception algorithms assumed that accurate location and pose information are available. In this paper, we propose a cooperative perception framework robust to the inaccurate location and pose, and we propose two methods to fuse objects into a unified coordinates.

The main contributions are summarized as follows:

- We propose an efficient and robust object-level coopera-

This work was supported in part by the National Key R&D Program of China under Grant 2021YFB1600402 and 2020YFB1600303 and in part by the State Key Laboratory of Automotive Safety and Energy Research Fund under Grant ZZ2021-023 and in part by Tsinghua University-Toyota Joint Center.

The authors are with the School of Vehicle and Mobility, Tsinghua University, Beijing, China (email:wenfuxi@tsinghua.edu.cn).

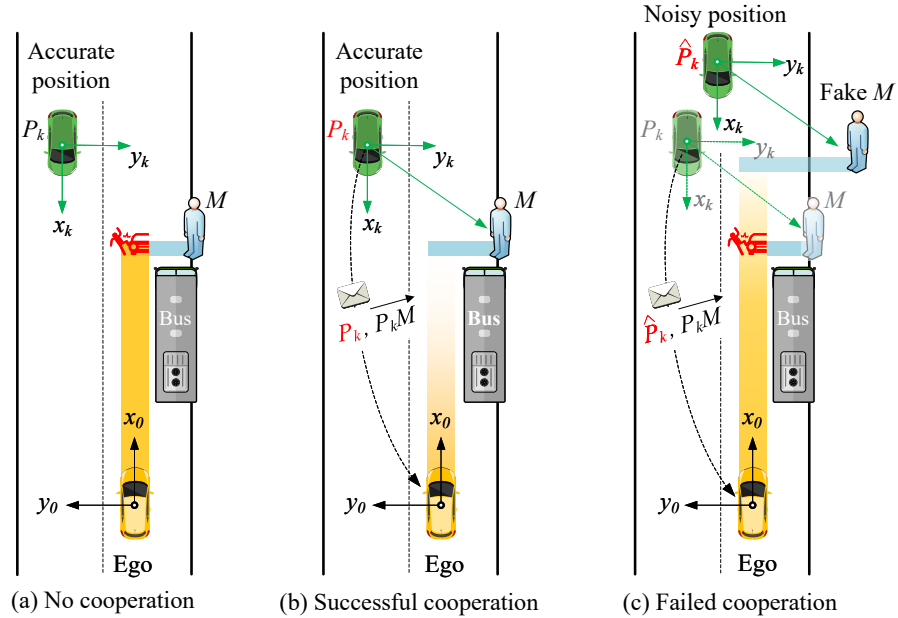


Fig. 1. **Illustration of cooperative perception.** (a) *No cooperation.* The Ego (yellow) might crash the pedestrian M because of occlusion of the bus (gray). (b) *Successful cooperation.* CAV_k sends its own accurate location P_k and the relative location of M to Ego. Crash might not happen. (c) *Failed cooperation.* CAV_k sends a noisy location \hat{P}_k to Ego, a fake M will appear from Ego's perspective. Crash might still happen.

tive perception framework for connected and automated driving.

- Iterative Closest Point (ICP)-based and Optimal Transport (OT)-based algorithms are developed to find the correspondence between the sets of the 3D bounding boxes representing the detected objects in different coordinates.
- The proposed algorithms outperform the state-of-the-art performance on benchmark dataset when location or heading errors occurred.

The rest of the paper is organized as follows: In Section II, the related work on cooperative perception and optimal transport are introduced. Section III contains the proposed object-level cooperative perception framework and two fusion algorithms. Numerical results are presented in Section IV, followed by conclusions in Section V.

II. RELATED WORK

A. Cooperative perception

In recent years, there has been an increasing interest in Cooperative driving [4], [5], [6]. Depending on cooperative agents, it can be classified into Vehicle-to-Vehicle (V2V) and Vehicle-to-Infrastructure (V2I). V2I has attracted a lot of interest of researchers [7], [8], [9], [10]. Our paper focuses on V2V cooperative perception, and the proposed algorithms can be also applied in V2I scenarios. As for V2V cooperative perception, recent studies primarily merge information from multiple CAVs at the feature level. F-Cooper [11] introduced feature-level data fusion to connected autonomous vehicles to enhance object detection. V2VNet [12] aggregated the feature information received from nearby vehicles to see through occlusions and detect long-range objects. OPV2V [13] released a large scale simulated V2V cooperation dataset, and presented

a benchmark with 16 implemented models, within which we implement our models. However, these existing studies are vulnerable to location and pose errors which are common and inevitable in real-world applications. FPV-RCNN [2] tried to introduce a location error correction module based on keypoints matching before feature fusion to make the model more robust, but it can not handle larger errors. Vadivelu *et al.* proposed a deep learning based framework to estimate potential errors [14], but they rely on feature-level fusion, which requires high computational capacity and is not general among different scenarios. In this paper, we try to take these errors into account, and design an efficient and robust object-level cooperative perception framework.

B. Optimal Transport Theory

The optimal transport theory was proposed by French geometer Gaspard Monge at the end of the 18th century for the first time [15]. In 2013, Cuturi [16] smoothed the classic optimal transport problem with an entropic regularization term and proposed a novel implementation of Sinkhorn's matrix scaling algorithm [17]. This makes the graphic processing unit (GPU) available for the optimal transport problem and accelerates its calculation much faster than conventional methods. In recent years, optimal transport has shown strong performance on several tasks with the rapid development of GPU. [18] presented a framework that generalizes the optimal transport problem in input spaces to (potentially) infinite-dimensional feature spaces. Sarlin *et al.* [19] formulated assignment of graph features as a differentiable optimal transport problem. [20] established the problem of finding dense correspondences across semantically similar images as an optimal transport problem. Qin *et al.* [21] applied optimal transport theory on

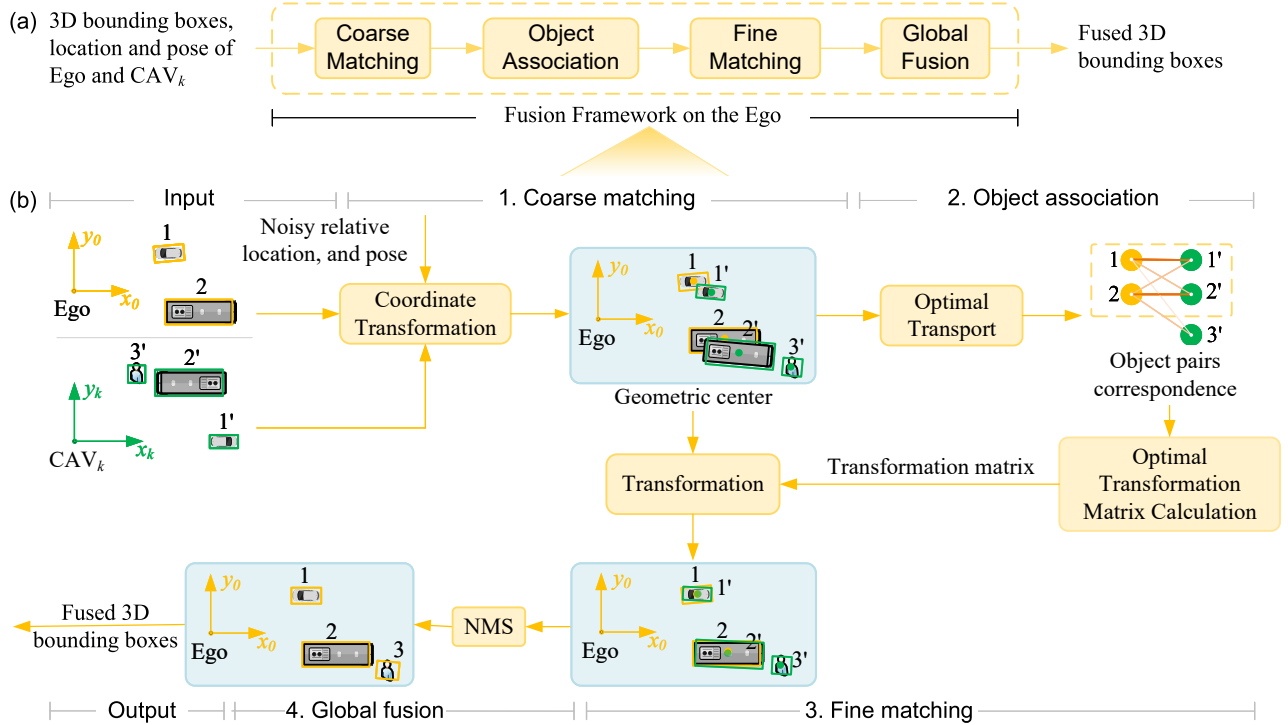


Fig. 2. **The architecture of the proposed cooperative perception fusion framework.** Each vehicle collects and processes data using on-board sensors and perception system, and produces a list of 3D bounding boxes representing the detected targets in the local coordinate. CAVs send their bounding boxes and their own location and pose to the Ego vehicle via the network. The Ego will calculate the relative transformation matrix and transform the received bounding boxes into Ego coordinate first in the *Coarse Matching* module. Next, the geometric centers of the two bounding boxes of the Ego's (yellow) and the received ones (green) are extracted as points. In the *Object Association* module, points representing the same targets in the real-world will be associated, and others will be filtered. Then, in the *Fine Matching* module, the remaining points are used to find a transformation matrix T , which is applied to the coarse matched results. Finally, the yellow and green points are merged using NMS. Fused 3D bounding boxes are generated for the downstream tasks of the Ego vehicle.

point cloud registration problem and developed a method with 100 times acceleration. For the simplicity and efficiency of optimal transport and Sinkhorn algorithm, we employ it to find the object correspondences between the Ego and CAVs.

III. PROPOSED APPROACH

A. System Framework

In this paper, we consider the vehicle-to-vehicle (V2V) communication setting, where each vehicle can broadcast and receive information to/from nearby vehicles within their communication range. We propose a distributed cooperative perception framework as shown in Fig. 2a. In a cooperative context, any connected vehicle can be the Ego vehicle to receive and fuse the information from other CAVs to improve its perception. Let $P_k = [x_k, y_k, z_k]^T$ be the real location of CAV $_k$ and $E_k = [\theta_k, \psi_k, \phi_k]^T$ be the pitch, roll and heading (yaw) angle, respectively. The measured location is

$$P_{\hat{k}} = [x_k + \delta_p, y_k + \delta_p, z_k + \delta_p]^T \quad (1)$$

where Gaussian noise $\delta_p \sim \mathcal{N}(0, \sigma_p)$. Without loss of generality, noiseless pitch and roll angles are considered [10], [12]. The measured pose is described as

$$E_{\hat{k}} = [\theta_k, \psi_k, \phi_k + \delta_\phi]^T \quad (2)$$

where Gaussian noise $\delta_\phi \sim \mathcal{N}(0, \sigma_\phi)$ is assumed. Here k and \hat{k} are used to distinguish the real and measured location and pose for CAV $_k$.

After data collection and object detection, CAV $_k$ produces a set of 3D bounding boxes $\mathcal{P}^k = \mathcal{P}^k$. Then $P_{\hat{k}}$ and $E_{\hat{k}}$, as well as the set \mathcal{P}^k are shared with Ego via V2V connections. These information will be fused with Ego's ($\mathcal{P}^0, P_0 = [x_0, y_0, z_0]^T$ and $E_0 = [\theta_0, \psi_0, \phi_0]^T$) in the proposed framework, cooperative and augmented perception $\mathcal{P} = \mathcal{O}^0 \cup \mathcal{O}^k$ is achieved, where \mathcal{O}^0 and \mathcal{O}^k denotes objects in Ego and CAV $_k$ coordinate, respectively.

As illustrated in Fig. 2, the proposed fusion framework is consisted of four modules: *Coarse Matching*, *Object Association*, *Fine Matching*, and *Global Fusion*.

- 1) In the *Coarse Matching* module, the Ego will first calculate the relative transformation matrix $\mathbf{T}_{\hat{k}}^0$ using $\{P_{\hat{k}}, E_{\hat{k}}\}$ and $\{P_0, E_0\}$, followed by transforming the received bounding boxes $\mathcal{P}^{\hat{k}}$ into Ego coordinate to formulate another set of \mathcal{Q}^0 .
- 2) For the *Object Association* module, the geometric centers of \mathcal{P}^0 and \mathcal{Q}^0 are extracted as point sets $\mathcal{P}_c^0 = \{p_1^0, \dots, p_M^0\} \in \mathbb{R}^{3 \times M}$ and $\mathcal{Q}_c^0 = \{q_1^0, \dots, q_N^0\} \in \mathbb{R}^{N \times 3}$. Points from the same targets will be associated, and others are temporarily ignored.
- 3) Then, in the *Fine Matching* module, the remaining points are used to find a transformation matrix, which is applied to the coarse matched results. For example, after *Coarse Matching*, green boxes $1', 2', 3'$ are converted to the vicinity of yellow boxes 1, 2, but not precisely aligned.

It's done in the *Object Association* and *Fine Matching* modules to recognize that 1 and 1' (2 and 2') are the same car (bus) in the real-world and estimate the transformation from set $\{1', 2', 3'\}$ to $\{1, 2\}$ (i.e., T_k^k).

- 4) Finally, the targets are merged in an Non-maximum suppression (NMS)[13], [22] style, fused 3D bounding boxes are generated for the downstream tasks of the Ego vehicle.

To find the association between objects and match them further, we propose two algorithms: Iterative Closest Point (ICP)-based and Optimal Transport theory (OT)-based. They are introduced in section III-B and III-C, respectively.

B. ICP-based framework

Mathematically, given \mathcal{P}_c^0 and \mathcal{Q}_c^0 , we intend to design an algorithm to find the common targets set $\hat{\mathcal{M}}$ (e.g., $\{(1, 1'), (2, 2')\}$ in Fig. 2) and align them to calculate the relative transformation T_k^k between the real and noisy location of CAV_k , i.e.,

$$\min_{\hat{\mathcal{M}}, T_k^k} \frac{1}{2} \sum_{(i,j) \in \hat{\mathcal{M}}} \left\| \begin{bmatrix} \mathbf{p}_j^0 \\ 1 \end{bmatrix} - \mathbf{T}_k^k \begin{bmatrix} \mathbf{q}_i^0 \\ 1 \end{bmatrix} \right\|_2^2 \quad (3)$$

s.t. $\mathbf{p}_j^0 \in \mathcal{P}_c^0$ and $\mathbf{q}_i^0 \in \mathcal{Q}_c^0$

where (i, j) is a possible object pair representing same target in the real world, transformation matrix \mathbf{T}_p^q is defined as

$$\mathbf{T}_p^q = \begin{bmatrix} \mathbf{R}_p^q & \mathbf{t}_p^q \\ 0 & 1 \end{bmatrix}, \quad (4)$$

and the coarse transformation matrix \mathbf{T}_k^0 can be calculated easily with the relative location and pose information between the Ego and the CAV_k as mentioned in section III-A.

Problem (3) can be solved by Iterative Closest Point (ICP) [23], which is one of the widely used algorithms for point cloud registration [24], [25], [26]. It finds the rigid transformation between source points and target points via iterative optimization and is guaranteed to converge to a locally optimal alignment [24]. In practice, a simple neighbour search algorithm is applied first to find the possible sets $\hat{\mathcal{M}}_1$ and $\hat{\mathcal{M}}_2$ that contains the common objects in \mathcal{P}_c^0 and \mathcal{Q}_c^0 , respectively. Then ICP is used on $\hat{\mathcal{M}}_1$ and $\hat{\mathcal{M}}_2$ to find $\hat{\mathcal{M}}$ and estimating the transformation matrix T_k^k , which is applied on \mathcal{Q}^0 , i.e., coarse matched bounding boxes of CAV_k . Finally, the 3D bounding boxes \mathcal{P}^0 and \mathcal{Q}^0 are aligned more accurately. The detailed algorithm is summarized in Algorithm 1.

C. OT-based framework

For neighbour selection step in Algorithm 1, parameter r need to be selected properly because it will directly influence the registration result (we set $r = 2m$). If r is too small, $\hat{\mathcal{M}}_1$ and $\hat{\mathcal{M}}_2$ will be empty. While if r is too large, a few outliers (i.e., those points with no correspondence), to which we empirically observed ICP being sensitive, will be contained. Under these, we propose a robust optimal transport (OT) based fusion algorithm as shown in Algorithm 2. The two methods will be compared and analyzed in section IV-B.

Algorithm 1 ICP-based Framework

Input: Centers of 3D bounding boxes of Ego and CAV_k , $\mathcal{P}_c^0 \in \mathbb{R}^{3 \times M}$ and $\mathcal{Q}_c^0 \in \mathbb{R}^{3 \times N}$;
Output: Transformation matrix T_k^k

▷ STEP 1: NEIGHBOUR SELECTION

- 1: **for** $i = 1, 2, \dots, M$ and $j = 1, 2, \dots, N$ **do**
- 2: **if** $\|\mathcal{P}_c^0(i) - \mathcal{Q}_c^0(j)\|_2 \leq r$ **then**
- 3: $\mathcal{P}_c^0(i) \in \hat{\mathcal{M}}_1, \mathcal{Q}_c^0(j) \in \hat{\mathcal{M}}_2$;
- 4: **end if**
- 5: **end for**

▷ STEP 2: POINT SET REGISTRATION

- 6: Calculate T_k^k using ICP with $\hat{\mathcal{M}}_1$ as the target points and $\hat{\mathcal{M}}_2$ as the source points.

Algorithm 2 OT-based Framework

Input: Centers of 3D bounding boxes of Ego and CAV_k , $\mathcal{P}_c^0 \in \mathbb{R}^{3 \times M}$ and $\mathcal{Q}_c^0 \in \mathbb{R}^{3 \times N}$;
Output: Transformation matrix T_k^k

▷ STEP 1: OPTIMAL TRANSPORT

- 1: **for** $i = 1, 2, \dots, M$ and $j = 1, 2, \dots, N$ **do**
- 2: Calculate $\mathbf{C}(i, j) = \|\mathcal{P}_c^0(i) - \mathcal{Q}_c^0(j)\|_2$
- 3: **end for**
- 4: $\bar{\mathbf{C}} = \mathbf{C}$;
- 5: $\bar{\mathbf{C}}(M+1, :) = \alpha \mathbf{1}_{N+1}$ and $\bar{\mathbf{C}}(:, N+1) = \alpha \mathbf{1}_{M+1}$;
- 6: Calculate assignment matrix $\bar{\mathbf{P}}$ using Sinkhorn;
- 7: $\mathbf{P} = \bar{\mathbf{P}}(:, :N)$;
- 8: Obtain $\hat{\mathcal{M}} = \{(o_i^p, o_j^q) \mid \mathbf{P}(i, j) = \text{argmax}_j \mathbf{P}(i, :) = \text{argmax}_i \mathbf{P}(:, j)\}$;

▷ STEP 2: RANDOM SAMPLING

- 9: **for** $s = 1, 2, \dots, n_s$ **do**
- 10: Random sample subset $\hat{\mathcal{M}}_s$ from $\hat{\mathcal{M}}$
- 11: Calculate $T_{k,s}^k$ on $\hat{\mathcal{M}}_s$ via SVD;
- 12: Apply $T_{k,s}^k$ to $\hat{\mathcal{M}}$, calculate matching ratio η_s ;
- 13: **end for**

▷ STEP 3: OPTIMAL TRANSFORMATION SELECTION

- 14: $s^* = \text{argmax}_{s=1,2,\dots,n_s} \eta(s)$ and $T_k^k = T_{k,s^*}^k$

To solve (3), the critical step is to find the common target set $\hat{\mathcal{M}}$ and assign pair-wise correspondence. Given two sets of the point representing the targets measured by Ego and CAV_k , it can be formulated as an optimal transport problem to minimize the transportation cost between source (points in \mathcal{P}_c^0) and target (points in \mathcal{Q}_c^0). For each point in \mathcal{P}_c^0 , we want to assign an unique correspondence from the point in \mathcal{Q}_c^0 . Similar to the graph matching task [19], two constraints should be satisfied: 1) a target in \mathcal{P}_c^0 can have at most one single correspondence in \mathcal{Q}_c^0 ; and 2) some targets will be unmatched because of different visions, occlusion, or detection errors.

We define a cost matrix $\mathbf{C} \in \mathbb{R}^{M \times N}$, to describe the transportation cost for association, where $\mathbf{C}(i, j)$ is the Euclidean distance between $\mathcal{P}_c^0(i)$ and $\mathcal{Q}_c^0(j)$. In order to propose a generalized formulation to handle the non-matched points, we follow [19], [27] augmenting \mathbf{C} to $\bar{\mathbf{C}}$ by appending a new row and column called dustbin, filled with a single hyperparameter

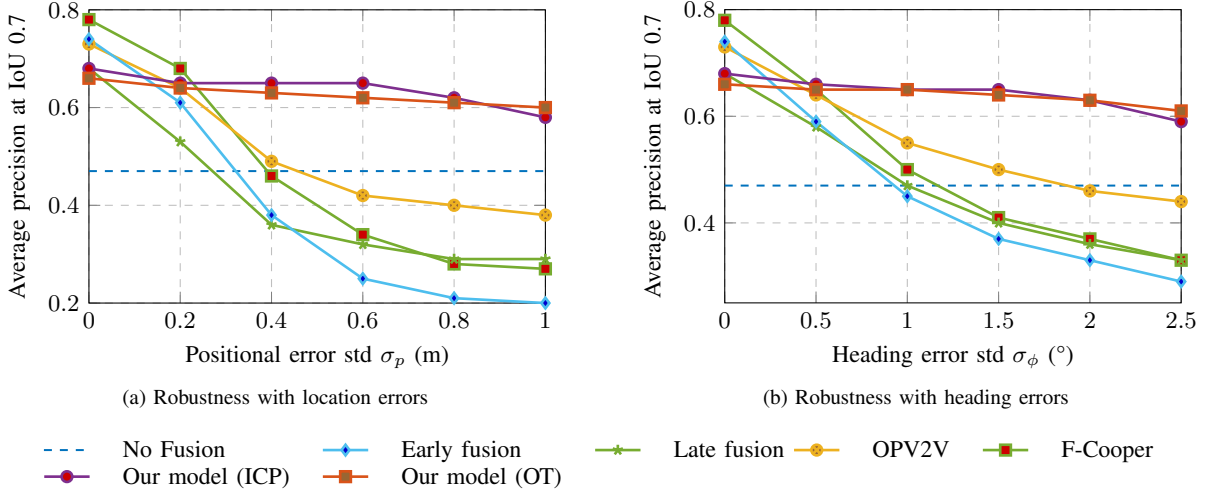


Fig. 3. Robustness assessment on *Test Culver City*

$\alpha \in \mathbb{R}$,

$$\bar{\mathbf{C}}(M+1, :) = \alpha \mathbf{1}_{N+1}^T \text{ and } \bar{\mathbf{C}}(:, N+1) = \alpha \mathbf{1}_{M+1} \quad (5)$$

Consequently, for each point in \mathcal{P}_c^0 , it is either matched to a point in \mathcal{Q}_c^0 or to the dustbin.

Once the cost matrix is defined, the task is to find the optimal assignment matrix $\bar{\mathbf{P}} \in \mathbb{R}^{(M+1) \times (N+1)}$, where $\bar{\mathbf{P}}(i, j)$ denotes the assignment probability on $\bar{\mathbf{C}}(i, j)$, then we have the following modified form of the optimal transport:

$$\begin{aligned} \max_{\bar{\mathbf{P}}} \quad & \sum_{i,j} -\bar{\mathbf{P}}(i, j) \bar{\mathbf{C}}(i, j) \\ \text{s.t.} \quad & \bar{\mathbf{P}} \mathbf{1}_{N+1} = [\mathbf{1}_M^T \ N]^T, \bar{\mathbf{P}}^T \mathbf{1}_{M+1} = [\mathbf{1}_N^T \ M]^T \end{aligned} \quad (6)$$

which can be solved efficiently on GPU by Sinkhorn algorithm [16].

Assignment matrix $\bar{\mathbf{P}}$ is constructed by dropping the last row and column of $\bar{\mathbf{P}}$, points $\mathcal{P}_c^0(i)$ and $\mathcal{Q}_c^0(j)$ are associated if $\bar{\mathbf{P}}(i, j) = \text{argmax}_i \bar{\mathbf{P}}(i, j) = \text{argmax}_j \bar{\mathbf{P}}(i, j)$, where $i \in [1, M]$ and $j \in [1, N]$. Set $\hat{\mathcal{M}} = \{(o_i^p, o_j^q)\}$ is consisted of all the possible point pairs $(\mathcal{P}_c^0(i), \mathcal{Q}_c^0(j))$.

It's worth noting that $\hat{\mathcal{M}}$ might be inaccurate due to outliers or noisy bounding box information. Random sampling techniques are utilized to further enhance the robustness of the proposed method. The procedure can be repeated n_s times or processed in parallel to find the best transformation matrix that maximizes the correctly matching ratio η . For the s th step, we randomly select a subset $\hat{\mathcal{M}}_s \subseteq \hat{\mathcal{M}}$, then estimate $T_{k,s}^{\hat{k}}$ using singular value decomposition (SVD). Applying $T_{k,s}^{\hat{k}}$ on all the point pairs (o_i^p, o_j^q) in $\hat{\mathcal{M}}$, if $\|o_i^p - T_{k,s}^{\hat{k}} o_j^q\|_2 \leq \tau$, it is regarded as an aligned pair. The aligned ratio η_s is calculated for the s th step. We set $\tau = 0.25m$ because we find that a simple late fusion system without object association can handle the location error whose Gaussian standard deviation (std) $\sigma_p \leq 0.2$, and tighter τ decreases the effect of random sampling. Optimal s^* is selected to maximize the correctly matching ratio, which is given by

$$s^* = \text{argmax}_{s=1,2,\dots,n_s} \eta_s. \quad (7)$$

Finally, $T_k^{\hat{k}} = T_{k,s^*}^{\hat{k}}$ is obtained that can be further applied on global fusion. The detailed algorithm is summarized in Algorithm 2.

IV. EXPERIMENTS

The proposed algorithms and benchmarks are evaluated on the OPV2V dataset [13]. OPV2V is an open dataset for perception with V2V communications. It contains 73 scenes collected utilizing CARLA simulator [28] and OpenCDA framework [29]. The dataset is organized as *Train*, *Validate*, and *Test* splits with 6764, 1981, and 2719 frames respectively. In order to narrow down the gap between simulation and real-world traffic, a digital town of Culver City, Los Angeles is built in [13]. These data (about 549 frames) are contained in the *Test* split, which is thus further grouped into *Default Test* and *Test Culver City* splits.

We train and validate the perception backbone on *Train* and *Validate* splits, then evaluate the fusion frameworks on *Default Test* and *Test Culver City* splits. The model is implemented in PyTorch [30], and runs on NVIDIA GTX 3090 GPU.

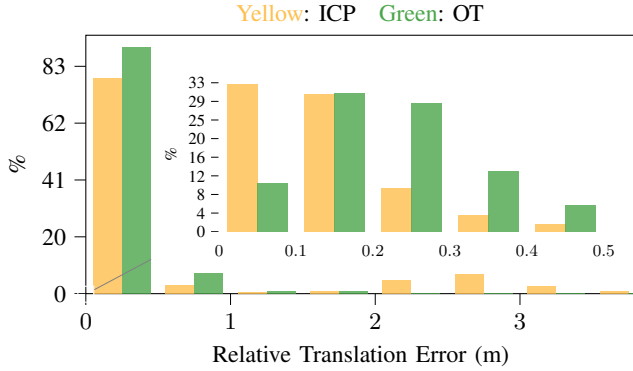
A. Robustness assessment

The proposed algorithms are compared with the mainstream early and late fusion methods, as well as the state-of-the-art (SOTA) intermediate fusion strategies, in terms of the robustness against the location and pose errors of the CAVs. According to the studies and experiments results shown in [10], intermediate fusion methods perform similar on location robustness. Therefore, F-Cooper [11] and OPV2V [13] are selected as the representative of SOTA intermediate fusion models. For fairness, all the compared methods use the same backbone PointPillars [31] and are implemented under the same framework proposed in [13].

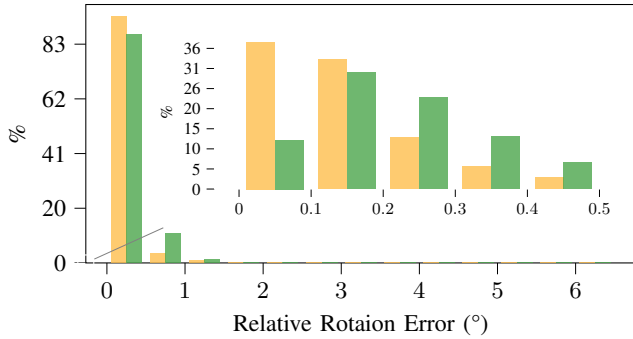
OPV2V dataset is collected via CARLA simulator, so it has accurate location and pose information of the Ego and CAVs. Hence, adding noise on the location and pose information of

the selected vehicles is easy. Furthermore, it is convenient to compare the results with ground truth.

The location and pose are described as $[x, y, z, \theta, \psi, \phi]$, where $[x, y, z]$ define the location, and $[\theta, \psi, \phi]$ are pitch, roll and heading (yaw) angles, respectively. In the following experiments, Gaussian noises $\delta_p \sim \mathcal{N}(0, \sigma_p)$ where $\sigma_p \in [0, 1]$ are added on the real location of the CAVs. Without loss of generality, $\delta_\phi \sim \mathcal{N}(0, \sigma_\phi)$ and $\sigma_\phi \in [0, 2.5]$ is added on the real heading angle. The standard deviation of the noise is uniformly sampled and the average precision (AP) is reported as the index for comparison.



(a) The distribution of RTE



(b) The distribution of RRE

Fig. 4. The distribution of RTE and RRE while $\sigma_p = 1m$

1) *Test Culver City*: Fig. 3 illustrates the numerical results on *Test Culver City*. The Ego vehicle senses the environment independently for no fusion case, therefore, the average precision of Intersection-over-Union (IoU) 0.7 is a constant and keeps stable at 0.47. For accurate location and heading scenarios (*i.e.*, $\sigma_p = 0$, $\sigma_\phi = 0$), early fusion outperforms late fusion, because the raw point clouds are utilized for fusion and less information is lost. Best performance is achieved for intermediate fusion models (*e.g.*, F-Cooper and OPV2V). Similar performance is observed for the proposed methods and the late fusion. While the performance of early fusion, late fusion, OPV2V and F-Cooper all decrease dramatically when the location or heading error occurred. The performance of F-Cooper drops below the no fusion method when $\sigma_p \geq 0.4m$ or $\sigma_\phi \geq 1^\circ$. While best performance is achieved for the proposed ICP and OT-based methods. Compared with OT-based method, slightly better performance is achieved for ICP-based method, but larger variations are also observed when

the levels of position and heading errors are increased. For OT based method, only 0.06 and 0.05 decrease respect to the accurate case when $\sigma_p = 1m$ and $\sigma_\phi = 2.5^\circ$.

2) *Default Test*: Test set *Default Test* is considered to further evaluate the robustness of the proposed methods. Table I and II show the AP at IoU 0.7 (AP70) of the models under different levels of σ_p and σ_ϕ on the test set *Default Test*. The average precision is higher than *Test Culver City* set because of the higher similarity to the training data.

The performance of the benchmarks is similar to the previous test set. It's worth noting that the proposed methods outperform the benchmarks with a large margin. Furthermore, the ICP based method is good at handling location errors, while OT-based method performs well with the heading errors. This is reasonable because the object association for ICP based method is achieved by searching neighbours within a given radius, which makes it robust to the errors caused by σ_p . For the proposed methods, only the set of 3D bounding boxes, location and pose of the CAVs are transmitted to Ego via the V2V connections. Therefore, the communication burden is low. Furthermore, they are efficient in terms of processing time, the proposed object association module takes only 5ms in average for each frame.

TABLE I
AP70 ON *Default Test*

Model	σ_p					
	0	0.2	0.4	0.6	0.8	1.0
No fusion	0.60	0.60	0.60	0.60	0.60	0.60
Early fusion	0.85	0.72	0.40	0.25	0.19	0.17
Late fusion	0.80	0.60	0.34	0.24	0.23	0.25
F-Cooper	0.82	0.74	0.49	0.32	0.23	0.19
OPV2V	0.82	0.74	0.58	0.49	0.44	0.42
Our model (ICP)	0.77	0.77	0.76	0.76	0.73	0.67
Our model (OT)	0.76	0.74	0.72	0.71	0.69	0.68

TABLE II
AP70 ON *Default Test*

Model	σ_ϕ					
	0	0.5	1.0	1.5	2.0	2.5
No fusion	0.60	0.60	0.60	0.60	0.60	0.60
Early fusion	0.85	0.72	0.54	0.42	0.36	0.30
Late fusion	0.80	0.64	0.47	0.38	0.32	0.29
F-Cooper	0.82	0.69	0.51	0.41	0.35	0.31
OPV2V	0.82	0.74	0.66	0.60	0.57	0.54
Our model (ICP)	0.77	0.77	0.76	0.71	0.67	0.62
Our model (OT)	0.76	0.75	0.74	0.73	0.72	0.70

B. Comparison of ICP and OT-based methods

As mentioned before, accurate location and pose information can be recorded in simulation environment. Therefore, we can compare the noisy transformation matrix $\hat{\mathbf{T}}_k^0 = \mathbf{T}_k^{\hat{k}} \mathbf{T}_k^0$ estimated by our algorithm with ground truth \mathbf{T}_k^0 to evaluate the calibration effect of the proposed models. For simplicity, we recover the $\hat{\mathbf{T}}_k^0$ back to a rotation matrix $\hat{\mathbf{R}}_k^0$ and a translation vector $\hat{\mathbf{t}}_k^0$ as in Eq. 4. Following [21], [32], two metrics are

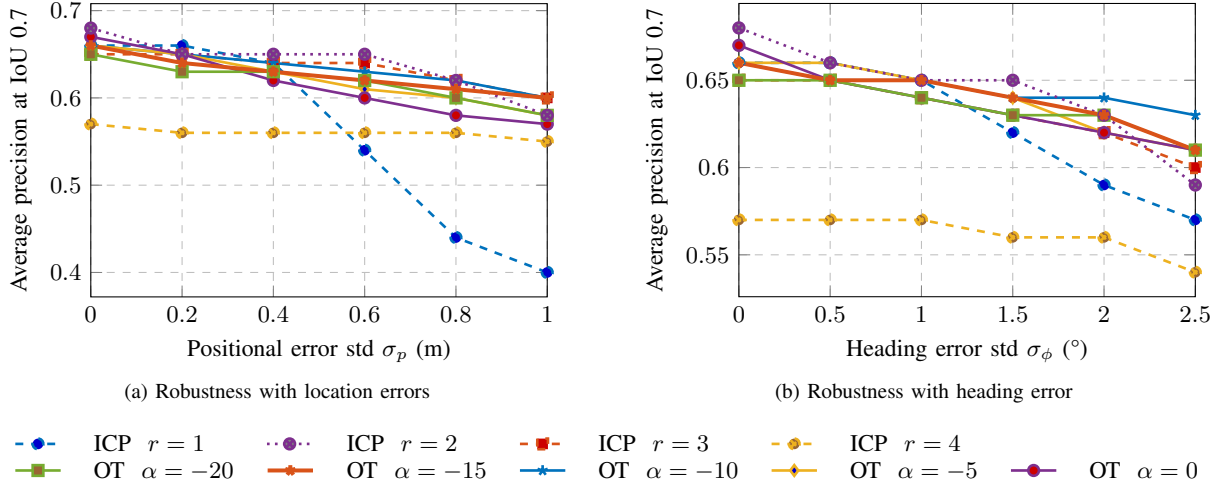


Fig. 5. The effect of hyperparameters

utilized to evaluate the difference between estimated results and ground truth.

- Relative Translation Error (RTE): Euclidean distance between the estimated and ground-truth translation vectors.

$$\text{RTE} = \|\hat{\mathbf{t}}_k^0 - \mathbf{t}_k^0\|_2 \quad (8)$$

- Relative Rotation Error (RRE): the geodesic distance between the estimated and ground-truth rotation matrices.

$$\text{RRE} = \arccos \left(\frac{\text{trace} \left((\mathbf{R}_k^0)^T \cdot \hat{\mathbf{R}}_k^0 \right) - 1}{2} \right) \quad (9)$$

For comparison, ICP and OT-based methods are implemented on the same *Test Culver City* set with $\sigma_p = 1m$. Excluding the frames with only one connected vehicle (*i.e.*, Ego), 478 frames are left for testing. For each frame, both RRE and RTE are calculated, the cumulative distribution results are shown in Fig.4a and Fig.4b, respectively.

As shown in Fig. 4a, the RTE of more than 90.6% of frames is smaller than 0.5m for OT-based method, which cuts the translation errors greatly. Furthermore, 1.9% of the frames has a larger RTE ($>1m$) for OT-based method, while for ICP-based method, the number is 17.6%. For ICP-based method, RTE of 64% of the frames is smaller than 0.2m, which is much higher than that of the OT-based method, which is 42%. That is the reason why ICP performs better overall in Table I. Furthermore, as shown in Fig. 4a and Fig. 4b, OT based method outperforms ICP when $\text{RTE} \in [0.1, 1]m$ and $\text{RRE} \in [0.2, 1]^\circ$. That is the reason why the slightly better robust performance is achieved for the OT-based method.

C. Hyperparameters

The radius of neighbour selection r and value of dutbin α are the hyperparameters of ICP and OT based method, respectively. To guarantee the generalization, the two parameters are selected on the *Train* set ($r = 2, \alpha = -15$), and applied on the *Default Test* and *Test Culver City* sets. To explore the

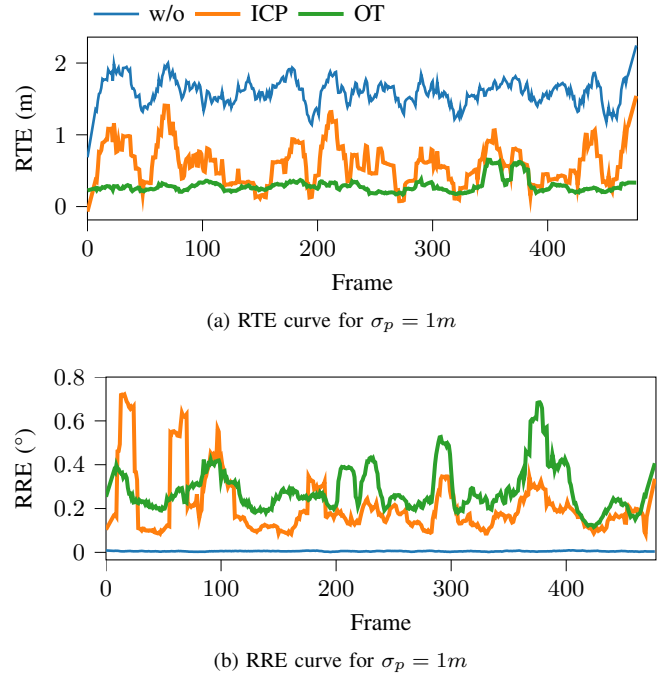
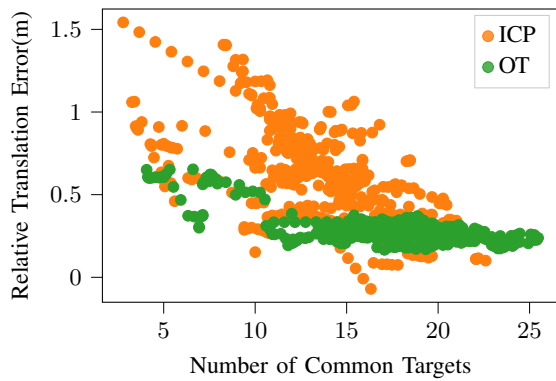


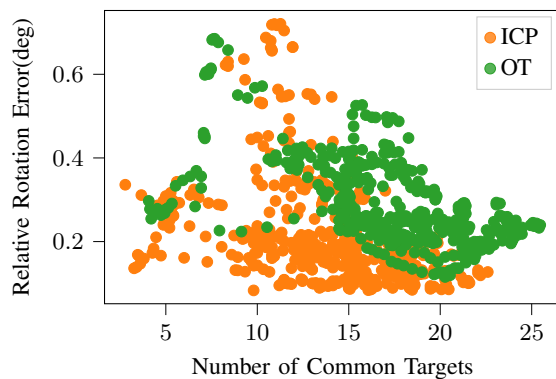
Fig. 6. RTE and RRE curve comparison

sensitivity of the proposed algorithm to hyperparameters, we illustrate the AP70 curve with respect to different levels of errors under various r and α in Fig.5.

It is interesting to observe that OT-based method is robust to parameter α , and similar performance is achieved with minor fluctuations. While for ICP-based method, besides the robustness, some changes happened when relative small or large r is selected. The number of targets within the common FOV is reduced for $r = 1$, therefore, performance degradation occurred. It drops to the level of the standard Late fusion method without calibration. For larger r value ($r = 4$), more outliers are introduced, that resulting in an overall deterioration in performance.



(a) Relative translation error vs NCT



(b) Relative rotation error vs NCT

Fig. 7. The effect of number of targets within the common field-of-view.

D. Limitations

The instant RTE and RRE curves over timestamps with $\sigma_p = 1m$ on *Test Culver City* are shown in Fig. 6a and Fig. 6b, respectively. The legend w/o is the results of vanilla late fusion without object association operation, the other two curves denote the filtered results of the proposed methods. It is interesting to observe that, lowest RTE is achieved for OT-based method, while slightly higher RRE is also occurred. This is because the 3D bounding boxes of the targets are realigned, but are impossible to be associated accurately due to the uncertainties in the detected bounding boxes, which suffer from information loss comparing to raw sensor data.

Same as the other cooperative perception techniques, common field-of-view (FOV) is required for the proposed methods, otherwise the system should degrade into non-cooperative mode. Here the number of common targets (NCT) is defined as the number of associated targets, after neighbor selection step in Algorithm 1 or optimal transport step in Algorithm 2. As illustrated in Fig. 7a and Fig. 7b, the performance of ICP-based methods is highly correlated with NCT, OT-based method relies less on it and performs more robust. It would be an interesting future work to further investigate the relationship, but beyond the scope of this paper.

V. CONCLUSIONS

We propose an efficient and robust object-level cooperative perception framework for connected and automated driving.

Efficiency is evaluated in terms of communication load and processing time because only the location, pose and 3D bounding boxes are required to share between Ego and CAVs. Furthermore, ICP and OT theory-based algorithms are developed to find the correspondence between the sets of the 3D bounding boxes. The proposed algorithms outperform the state-of-the-art performance on benchmark datasets when location or heading errors occur, which is common and inevitable in real-world applications. While the performance of ICP and OT-based methods are dependent on the number of targets within the common FOV.

REFERENCES

- [1] B. Xu, S. E. Li, Y. Bian, S. Li, X. J. Ban, J. Wang, and K. Li, "Distributed conflict-free cooperation for multiple connected vehicles at unsignalized intersections," *Transportation Research Part C: Emerging Technologies*, vol. 93, pp. 322–334, 2018.
- [2] Y. Yuan, H. Cheng, and M. Sester, "Keypoints-based deep feature fusion for cooperative vehicle detection of autonomous driving," *IEEE Robotics and Automation Letters*, vol. 7, no. 2, pp. 3054–3061, 2022.
- [3] H. Pei, J. Zhang, Y. Zhang, X. Pei, S. Feng, and L. Li, "Fault-tolerant cooperative driving at signal-free intersections," *IEEE Transactions on Intelligent Vehicles*, pp. 1–1, 2022.
- [4] Z. Wang, K. Han, and P. Tiwari, "Digital twin-assisted cooperative driving at non-signalized intersections," *IEEE Transactions on Intelligent Vehicles*, 2021.
- [5] C. Chen, Q. Xu, M. Cai, J. Wang, J. Wang, and K. Li, "Conflict-free cooperation method for connected and automated vehicles at unsignalized intersections: Graph-based modeling and optimality analysis," *IEEE Transactions on Intelligent Transportation Systems*, pp. 1–18, 2022.
- [6] J. Cui, H. Qiu, D. Chen, P. Stone, and Y. Zhu, "Coopernaut: End-to-end driving with cooperative perception for networked vehicles," in *IEEE/CVF Conference on Computer Vision and Pattern Recognition (CVPR)*, 2022.
- [7] Y. Li, S. Ren, P. Wu, S. Chen, C. Feng, and W. Zhang, "Learning distilled collaboration graph for multi-agent perception," in *Advances in Neural Information Processing Systems*, A. Beygelzimer, Y. Dauphin, P. Liang, and J. W. Vaughan, Eds., 2021.
- [8] Y. Li, D. Ma, Z. An, Z. Wang, Y. Zhong, S. Chen, and C. Feng, "V2X-Sim: Multi-agent collaborative perception dataset and benchmark for autonomous driving," *IEEE Robotics and Automation Letters*, vol. 7, no. 4, pp. 10914–10921, 2022.
- [9] H. Yu, Y. Luo, M. Shu, Y. Huo, Z. Yang, Y. Shi, Z. Guo, H. Li, X. Hu, J. Yuan, and Z. Nie, "Dair-v2x: A large-scale dataset for vehicle-infrastructure cooperative 3d object detection," in *Proceedings of the IEEE/CVF Conference on Computer Vision and Pattern Recognition (CVPR)*, June 2022, pp. 21 361–21 370.
- [10] R. Xu, H. Xiang, Z. Tu, X. Xia, M.-H. Yang, and J. Ma, "V2X-ViT: Vehicle-to-everything cooperative perception with vision transformer," in *Proceedings of the European Conference on Computer Vision (ECCV)*, 2022.
- [11] Q. Chen, X. Ma, S. Tang, J. Guo, Q. Yang, and S. Fu, "F-cooper: Feature based cooperative perception for autonomous vehicle edge computing system using 3D point clouds," in *Proceedings of the 4th ACM/IEEE Symposium on Edge Computing*, ser. SEC '19. New York, NY, USA: Association for Computing Machinery, 2019, p. 88–100.
- [12] T.-H. Wang, S. Manivasagam, M. Liang, B. Yang, W. Zeng, and R. Urtasun, "V2VNet: Vehicle-to-vehicle communication for joint perception and prediction," in *Computer Vision – ECCV 2020: 16th European Conference, Glasgow, UK, August 23–28, 2020, Proceedings, Part II*. Berlin, Heidelberg: Springer-Verlag, 2020, p. 605–621.
- [13] R. Xu, H. Xiang, X. Xia, X. Han, J. Li, and J. Ma, "OPV2V: An open benchmark dataset and fusion pipeline for perception with vehicle-to-vehicle communication," in *2022 IEEE International Conference on Robotics and Automation (ICRA)*, 2022.
- [14] N. Vadivelu, M. Ren, J. Tu, J. Wang, and R. Urtasun, "Learning to communicate and correct pose errors," *arXiv preprint arXiv:2011.05289*, 2020.
- [15] C. Villani, *Optimal transport: old and new*. Springer, 2009, vol. 338.
- [16] M. Cuturi, "Sinkhorn distances: Lightspeed computation of optimal transport," *Advances in neural information processing systems*, vol. 26, 2013.

- [17] R. Sinkhorn, “Diagonal equivalence to matrices with prescribed row and column sums,” *The American Mathematical Monthly*, vol. 74, no. 4, pp. 402–405, 1967.
- [18] Z. Zhang, M. Wang, and A. Nehorai, “Optimal transport in reproducing kernel hilbert spaces: Theory and applications,” *IEEE transactions on pattern analysis and machine intelligence*, vol. 42, no. 7, pp. 1741–1754, 2019.
- [19] P.-E. Sarlin, D. DeTone, T. Malisiewicz, and A. Rabinovich, “Superglue: Learning feature matching with graph neural networks,” in *Proceedings of the IEEE/CVF conference on computer vision and pattern recognition*, 2020, pp. 4938–4947.
- [20] Y. Liu, L. Zhu, M. Yamada, and Y. Yang, “Semantic correspondence as an optimal transport problem,” in *IEEE/CVF Conference on Computer Vision and Pattern Recognition (CVPR)*, 2020, pp. 4462–4471.
- [21] Z. Qin, H. Yu, C. Wang, Y. Guo, Y. Peng, and K. Xu, “Geometric transformer for fast and robust point cloud registration,” in *Proceedings of the IEEE/CVF Conference on Computer Vision and Pattern Recognition*, 2022, pp. 11 143–11 152.
- [22] N. Bodla, B. Singh, R. Chellappa, and L. S. Davis, “Soft-NMS — improving object detection with one line of code,” *IEEE International Conference on Computer Vision (ICCV)*, pp. 5562–5570, 2017.
- [23] P. Besl and N. D. McKay, “A method for registration of 3-D shapes,” *IEEE Transactions on Pattern Analysis and Machine Intelligence*, vol. 14, no. 2, pp. 239–256, 1992.
- [24] J. Zhang, Y. Yao, and B. Deng, “Fast and robust iterative closest point,” *IEEE Transactions on Pattern Analysis and Machine Intelligence*, vol. 44, no. 7, pp. 3450–3466, 2022.
- [25] S. Rusinkiewicz, “A symmetric objective function for ICP,” *ACM Transactions on Graphics*, vol. 38, no. 4, jul 2019.
- [26] A. L. Pavlov, G. W. Ovchinnikov, D. Y. Derbyshev, D. Tsetserukou, and I. V. Oseledets, “AA-ICP: Iterative closest point with anderson acceleration,” in *2018 IEEE International Conference on Robotics and Automation (ICRA)*, 2018, pp. 3407–3412.
- [27] D. DeTone, T. Malisiewicz, and A. Rabinovich, “Superpoint: Self-supervised interest point detection and description,” in *Proceedings of the IEEE Conference on Computer Vision and Pattern Recognition (CVPR) Workshops*, June 2018.
- [28] A. Dosovitskiy, G. Ros, F. Codevilla, A. Lopez, and V. Koltun, “Carla: An open urban driving simulator,” in *Conference on robot learning*. PMLR, 2017, pp. 1–16.
- [29] R. Xu, Y. Guo, X. Han, X. Xia, H. Xiang, and J. Ma, “Openeda: an open cooperative driving automation framework integrated with co-simulation,” in *2021 IEEE International Intelligent Transportation Systems Conference (ITSC)*. IEEE, 2021, pp. 1155–1162.
- [30] A. Paszke, S. Gross, S. Chintala, G. Chanan, E. Yang, Z. DeVito, Z. Lin, A. Desmaison, L. Antiga, and A. Lerer, “Automatic differentiation in pytorch,” *NIPS Workshop*, 2017.
- [31] A. H. Lang, S. Vora, H. Caesar, L. Zhou, J. Yang, and O. Beijbom, “Pointpillars: Fast encoders for object detection from point clouds,” in *Proceedings of the IEEE/CVF Conference on Computer Vision and Pattern Recognition (CVPR)*, June 2019.
- [32] Z. J. Yew and G. H. Lee, “Rpm-net: Robust point matching using learned features,” in *2020 IEEE/CVF Conference on Computer Vision and Pattern Recognition (CVPR)*, 2020, pp. 11 821–11 830.